J Supercond Nov Magn
DOI 10.1007/s10948-017-4054-0

ORIGINAL PAPER

Enhancing the Magnetic Properties of Li-Sb Ferrites

Ebtesam E. Ateia[1] · G. Abdelatif[1] · M. A. Ahmed[1] · M. Abd Alla Mahmoud[1]

Received: 8 November 2016 / Accepted: 13 March 2017

Abstract A series of $Li_{0.5+z}Sb_zLa_xFe_{2.5-2z-x}O_4$ spinel ferrites were prepared by a standard ceramic technique. All samples sintered at 1100 °C with a heating rate of 4 °C/min. A single-phase cubic spinel structure was confirmed by X-ray diffraction analysis with the appearance of small peaks that represent secondary phases. AC conductivity as a function of frequency and temperature was carried out. The calculated values of the activation energy approve the obtained results and indicate the semiconductor properties of the investigated samples. Due to large ionic radius, La^{3+} ions cannot completely substitute Fe^{3+} ions. These ions occupy grain boundaries instead of spinel lattice and form secondary phases after interaction with other ions present in grain boundaries. The magnetic parameters were calculated from the magnetic susceptibility data, in the temperature range 300–900 K at three different magnetic field intensities of 2160, 3000, and 3800 Oe. The data showed a decrease in the magnetic susceptibility till it reaches the Curie temperature (T_C). The observed decrease in the Curie temperature with La content was explained on the basis of Neel's model and the cation distribution. One recommends the use of such sample in the application that demands high resistivity and high Curie temperature.

Keywords Rare earth ions · Electrical measurements · Standard ceramic technique · Antimony ferrite

✉ Ebtesam E. Ateia
drebtesam2000@yahoo.com

[1] Physics Department, Faculty of Science, Cairo University, Giza, Egypt

1 Introduction

Among the substituted ferrites, lithium ferrites form an important class and are the most widely studied. This is because of their distinguishing qualities like high Curie temperature, square hysteresis loop, high resistivity, low dielectric loss, and wide and adjustable range of saturation magnetization. They have wide industrial and technological applications and are extensively studied by various workers [1]. The optimum suitable ferrite for a particular application can be obtained by making various substitutions like Sb, Co, Mn, Al, Cr, Ga, and Ti. However, only few workers have reported on the Sb^{3+}-substituted Li ferrite. The Li^{1+} ion tends to occupy the B site, but above $x = 0.5$, it starts drifting to the A site, while the Sb^{5+} ions have preference for the B site [2].

Dhanaraju et al. [3] studied Sb^{5+}-doped copper ferrite. The substitution of Sb^{5+} led to the increase of domain wall energy. Low concentration of substituent with the increased domain wall energy was suitable to induce a driving force for the movement of grain boundary resulting in an increase in grain size.

Antimony tin oxide (ATO) nanoparticles doped with different Sb contents was studied by Zhang et al. [4]. The results showed that the crystallinity of the powders decreased with the doping of Sb. The widening phenomenon of diffraction peaks appeared when the mole ratio of Sb to Sn is 2:10. This can be attributed to the lattice defect caused by Sb content.

The aim of the present work is to study the effect of La^{3+} ions on the electrical and magnetic properties of Li-Sb ferrites. The modification of the magnetic and electric properties could be led to several technological applications like fluid technology, high-density magnetic recording,

Published online: 31 March 2017

magnetic resonance imaging, data storage, and photovoltaic applications [5–7]. This study is also carried out to select the suitable materials for specific applications.

2 Experimental Work

The ferrite samples were prepared using standard ceramic techniques [8]. Analar grade oxides (BDH) were mixed in stoichiometric ratio according to the formula $Li_{0.5+z}Sb_zR_xFe_{2.5-2z-x}O_4$. Grinding using an agate mortar for 4 h was carried out for each sample. The mixture was transferred to an electric shaker and ball milled for another 4 h. After that, they were pressed into pellet form using a pressure of 5×10^8 N m^{-2}. The presintering was carried out at 800 °C in air using a Lenton furnace, type UAF 16/5 (England), for 10 h and sintered at 1100 °C with a heating rate of 4 °C min^{-1}. The samples were cooled to room temperature with the same rate as that of heating.

The AC conductivity (σ) was measured using a self-calibrated Hioki LCR Hi tester, type 3530 (Japan), as a function of temperature from 300 to 750 K at a frequency ranging from 100 kHz to 5 MHz. X-ray diffraction patterns were obtained by using a Diano X-ray diffractometer. The magnetic susceptibility was measured by Faraday's method balance [9, 10].

3 Results and Discussion

Figure 1 shows the X-ray diffractograms for ferrite samples of the general formula $Li_{0.5+z}Sb_zLa_xFe_{2.5-2z-x}O_4$ with $z = 0.1$ and $(0.1 \leq x \leq 0.7)$. The diffraction peaks corresponding to planes (111), (220), (311), (222), (400), (422), (511), (440), (620), and (533) provide a clear evidence for the formation of spinel structure with the appearance of small peaks that represent secondary phases at $x \geq 0.3$. This can be attributed to the large ionic radius of La^{3+} (1.15 Å) ion which prevents it from occupying the tetrahedral and the octahedral sites [11] and forming aggregates on the grain boundary. As La^{3+} ion content increases, the aggregates increase and, as a result, further compression in the spinel lattice will occur. It is possible that the spinel lattice is compressed by the intergranular secondary phase due to the differences in the thermal expansion coefficients [12].

Generally, the solubility limit of the rare earth ions depends on the method of synthesis, ionic radii, and thermal treatment given to ferrite. In our case, rare earth ion possesses larger ionic radii than Li^{1+}, Sb^{3+}, and Fe^{3+} ions, and these ions produce impure phases in spinel lattice [13].

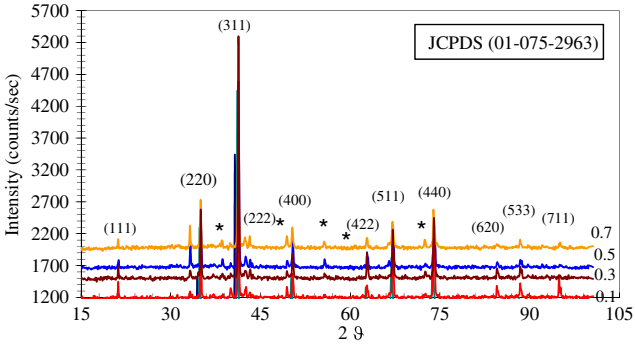

Fig. 1 The x-ray diffraction pattern for $Li_{0.5+z}Sb_zLa_xFe_{2.5-2z-x}O_4$, $(z = 0.1,\ 0.1 \leq x \leq 0.7)$

Figure 2a–d correlates Lnσ ($\sigma\,\Omega^{-1}$ cm^{-1}) versus $1000/T$ (K^{-1}) for the samples $Li_{0.5+z}Sb_zLa_xFe_{2.5-2z-x}O_4$ $(0.1 \leq x \leq 0.7,\ z = 0.1)$ in the frequency range 10 kHz–5 MHz. The general behavior of conductivity data is the existence of two straight lines at each frequency, intersecting at a point slightly affected by the La content.

In the present study, Fe^{3+} ions are partially replaced by La^{3+} ions. The rare earth ions (La^{3+}) have a strong preference to occupy the B sites, leading to the replacement of Fe^{3+} ions. In other words, the La^{3+} ions do not participate in the conduction process but limit the degree of $Fe^{2+} \leftrightarrow Fe^{3+}$ conduction by blocking up the $Fe^{2+} \leftrightarrow Fe^{3+}$ transformation [14]. This phenomenon impedes the Verwey–de Boer mechanism between the distributed Fe^{2+} and Fe^{3+} ions at the equivalent crystallographic lattice sites, causing an increase in the resistivity.

The Fe^{2+} ions may be also formed due to partial evaporation of lithium during the sintering process, and they preferentially occupy the octahedral sites [2].

The change in the slopes of the investigated samples is attributed to the change in the conduction mechanism. The conduction at lower temperature (below Curie temperature) is due to hopping of electrons between Fe^{2+} and Fe^{3+} ions and jumping of holes between Sb^{5+} and Sb^{3+}, while that at higher temperature (above Curie temperature) is due to polaron hopping. Figure 2 and Table 1 show that the activation energy in the high-temperature region (E_{II}) is greater than that in the low-temperature one. This can be attributed to the role of high temperature on the lattice vibrations and the generation of phonons. These disturb the system, and one needs more thermal energy for the charge carriers to jump between the different conduction states.

Figure 3a–d correlates the molar magnetic susceptibility and absolute temperature as a function of a magnetic field intensity for samples $Li_{5.0+z}La_xSb_zFe_{2.5-2z-x}O_4$ where $z = 0.1$ and $0.1 \leq x \leq 0.7$. From the figure, it is clear that χ_M decreases with increasing temperature and then

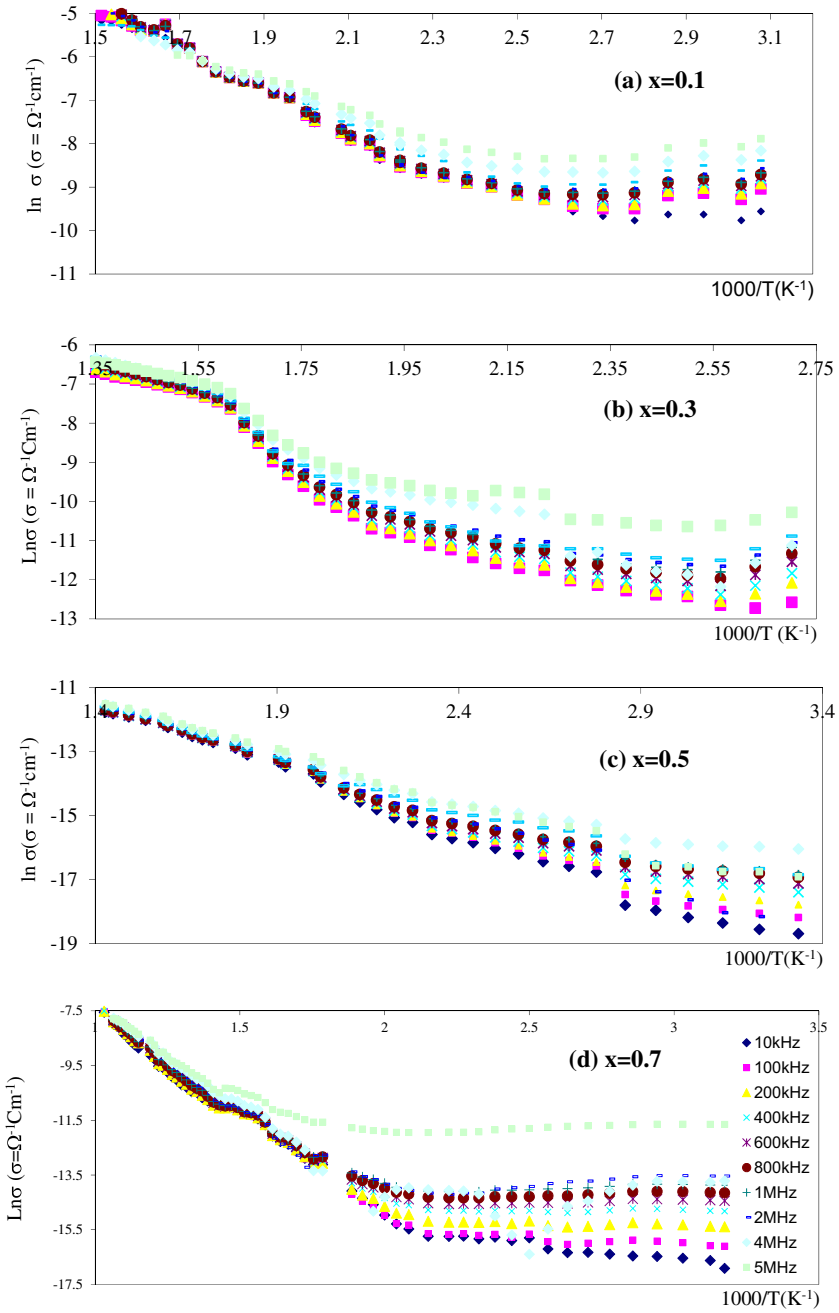

Fig. 2 **a–d** Relation between ac-electrical conductivity and reciprocal of absolute temperature at different frequencies for the samples $Li_{0.5+z}Sb_zLa_xFe_{2.5-2z-x}O_4$, $(z = 0.1,\ 0.1 \leq x \leq 0.7)$

decreases drastically to reach its minimum value. This is a well-known behavior and was explained in the previous work [15]. The investigated samples Sb^{3+} (0.62 Å), Li^{1+} (0.68 Å), and La^{3+} ions are non-magnetic and do not contribute to the magnetization. Thus, the magnetic moment is due only to Fe ion concentration.

The obtained data shows that the magnetic susceptibility χ_M increases with increasing La^{3+} ion concentration, giving a maximum at $x = 0.7$. This can be interpreted due to the redistribution of Fe^{3+} ions among tetrahedral (A) and octahedral (B) sites. However, some of Fe^{3+} with magnetic moment (5 Bohr magneton (BM)) migrates from B to A sites and transformed to Fe^{2+} with lower magnetic moment (3 BM), while the magnetic moment of La^{3+} is almost negligible [13]. Hence, M_A is decreased, giving rise to a maximum net magnetization. On the other side, the local magnetic moment of Fe^{3+} on the B site is higher than that on the A site which implies a stronger covalence on the A site than that on the B site [16]. Other factors which must be taken also into account are spin-orbit coupling

Table 1 the values of activation energy at low temperature region (E_I), at high temperature region (E_I) and at different frequencies for $Li_{0.5+z}Sb_zLa_xFe_{2.5-2z-x}O_4$

Freq. (kHz)	E_I(eV) x=0.1	E_{II}(eV) x=0.1	E_I(eV) x=0.3	E_{II}(eV) 3 x=0.3	E_I(eV) x=0.5	E_{II}(eV) x=0.5	E_I(eV) x=0.7	E_{II}(eV) x=0.7
100	0.30	0.73	0.56	0.84	0.58	0.67	0.79	0.89
200	–	0.85	0.46	1.02	–	0.82	–	0.82
400	0.20	0.85	0.17	0.48	0.25	0.65	0.77	0.97
600	0.25	0.70	0.13	0.00	0.20	0.55	–	0.95
800	0.22	0.55	0.18	0.69	0.25	0.50	–	0.91
1000	–	0.49	0.40	048	0.39	0.48	–	0.90

and $3d$-$4f$ coupling. Spin-orbit coupling effect dominates in RE ions [17], while $3d$-$4f$ interaction regulates the magnetic and electrical properties of the prepared ferrite samples.

The obtained data obeys the well-known Curie–Weiss law where $1/\chi$ varies linearly with temperature in the paramagnetic region. The values of the Curie constant (C) and the effective magnetic moment (μ_{eff}) are calculated

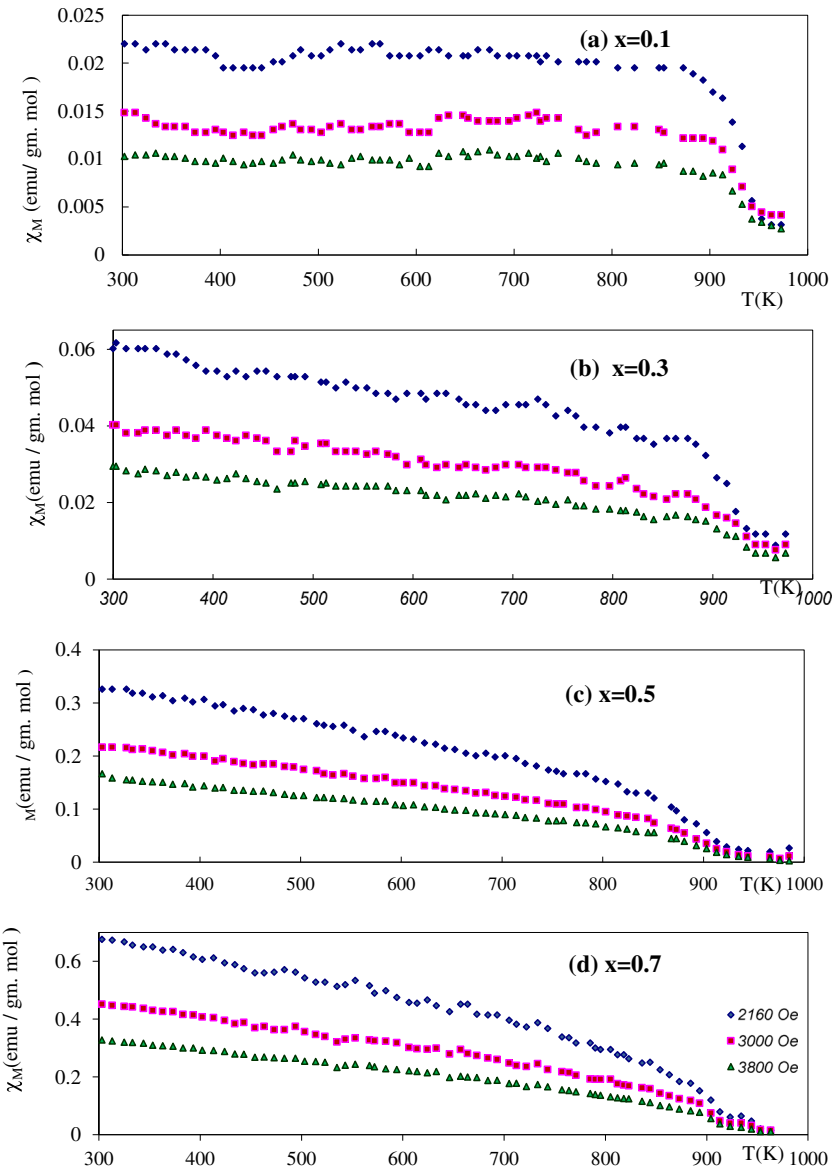

Fig. 3 **a–d** Relation between the molar magnetic susceptibility and absolute temperature for ferrite samples $Li_{0.5+z}Sb_zLa_xFe_{2.5-2z-x}O_4$, where $(0.1 \leq x \leq 0.7,\ z = 0.1)$ sintered at rate 4 °C/min at different magnetic field intensities

Table 2 Magnetic constants: Curie constant(C), effective magnetic moment (μ_{geff}), Curie- Weiss constant (θ) at different La ion concentration

H(Oe)	C	μ_{geff}(BM)	θ(K)	C	μ_{geff}(BM)	θ(K)
	$X = 0.1$			$X = 0.3$		
2160	1.039	2.885	840	2.286	4.279	820
3000	0.774	2.441	840	2.128	4.180	780
3800	0.546	2.091	840	1.867	3.867	760
	$X = 0.5$			$X = 0.7$		
2160	2.955	4.864	840	3.462	5.266	870
3000	2.406	4.391	830	2.632	4.591	860
3800	2.308	4.299	830	2.326	4.316	855

from the reciprocal of magnetic susceptibility with absolute temperature (not present here) using the following equation [18].

$$C = \frac{1}{\text{slope}}, \quad \mu_{\text{eff}} = 2.83\sqrt{C} \tag{1}$$

The Curie–Weiss constant (θ) is calculated from the intercept of the straight line with the temperature axis. The experimental data is fitted linearly, and the magnetic parameters are calculated and tabulated in Table 2. The experimental C values provide information on the number of unpaired electrons in the investigated system.

The Curie temperature (T_C) decreases with increasing La^{3+} ion concentration as shown in Fig. 4a. The variation of Curie temperature (T_C) is explained on the basis of A–B interactions. The addition of Sb^{3+}, Li^{1+}, and La^{3+} ions either onto A or B site weaken the A–B interaction and lowers the Curie temperature. According to Neel's molecular field theory, the A–B exchange interaction is stronger than A–A or B–B exchange interactions [18]. In other words, the replacement of Fe^{3+} magnetic ion by diamagnetic ions reduces the number of magnetic linkage and consequently decreases the Curie temperature. A decrease of T_C with substituent concentration (x) in this study is similarly observed [3] (Fig. 4a).

The exchange interaction constant (J) is calculated for the investigated samples using the following equation [19]:

$$J = \frac{3kT_C}{2ZS(S+1)} \tag{2}$$

where k is the Boltzmann constant, T_C is the Curie temperature, Z is the number of nearest neighbors of the atom, and S is the spin magnetic moment of the atoms. The obtained data reveals that J decreases with increasing La ion concentration (as shown in Fig. 4b). This means that La^{3+} ions reduce all magnetic parameters as shown in Fig. 4a–b and Table 2.

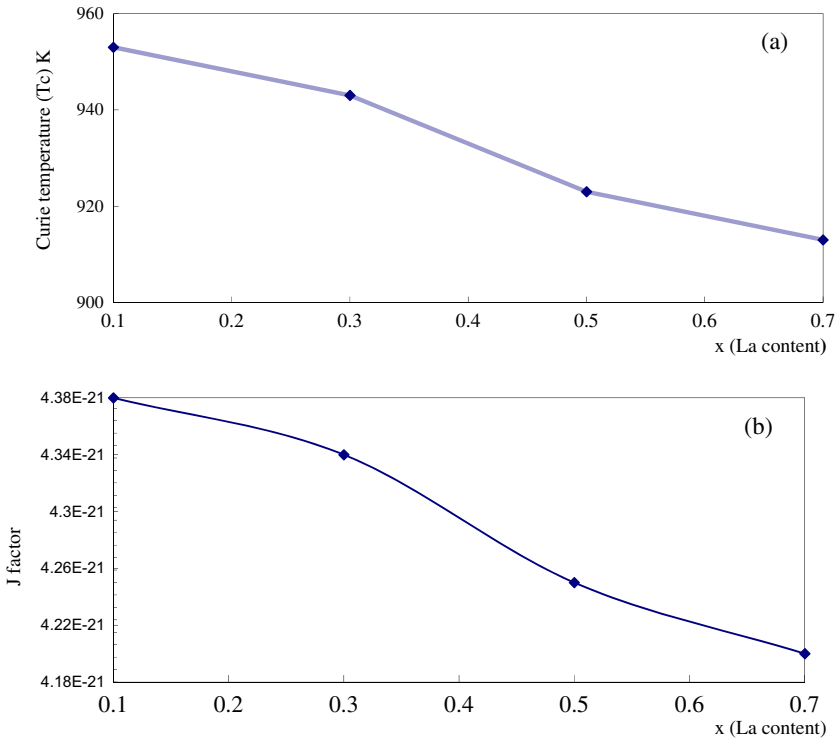

Fig. 4 Relation between (**a**) La content and Curie temperature and (**b**) La content and the exchange interaction constant (J) for $Li_{0.5+z}Sb_zLa_xFe_{2.5-2z-x}O_4$; $0.1 \leq x \leq 0.7$ sintered at 1100 °C with the rate of heating 4 °C/min

4 Conclusion

The composition $Li_{0.5+z}Sb_zLa_xFe_{2.5-2z-x}O_4$, $z = 0.1$, and $0.1 \leq x \leq 0.7$ showed a spinel structure with small secondary phase at $x \geq 0.3$.

The molar magnetic susceptibility (w_M) decreases with the temperature before it drops to the critical temperature (T_C).

From the obtained data, one prefers the sample of $y = 0.7$ as the optimum La^{3+} concentration due to its favorable magnetic properties and high resistivity.

High value of resistivity makes this ferrite suitable for the high frequency applications where eddy current losses become appreciable.

References

1. Verma, S., Joy, P.A.: Magnetic properties of super paramagnetic lithium ferrite nanoparticles. J. Appl. Phys. **98** (2005). doi:10.1063/1.2149493
2. Radhapiyari, L., Phanjoubam, S., Sarma, H.N.K., Prakash, C.: Influence of Co^{2+} on the electrical and magnetic properties of Li–Sb ferrites. Mater. Lett. **44**, 65–69 (2000)
3. Dhanaraju, R., Rajua, M.K., Brahmajirao, V., Bangarraju, S.: Studies on Curie temperature in relation to the magnetic and electrical properties Zn and Sb substituted Cu ferrites. Int. J. Sci. Technol. **1**(5), 253–263 (2012)
4. Zhang, J., Wang, L.-X., Liang, M.-P., Zhang, Q.-T.: Effects of Sb content on structure and laser reflection performance of ATO nanomaterials. Trans. Nonferrous Met. Soc. China **24**, 131–135 (2014)
5. Butt, F.K., Bandarenka, A.S.: Microwave-assisted synthesis of functional electrode materials for energy applications. J. Solid State Electrochem. **20**, 2915–2928 (2016)
6. Butt, F.K., Cao, C., Idrees, F., Tahir, M., Hussain, R., Ahmed, R., Khan, W.S., Hussain, R., Ahmed, R., Khan, W.S.: Novel $Zn_2V_2O_7$ hierarchical nanostructures: Optical and hydrogen storage properties. Int. J. Hydrog. Energy **xxx** (2015). doi:10.1016/j.ijhydene.2015.05.086
7. Butt, F.K., Mirza, M., Cao, C., Idrees, F., Tahir, M., Safdar, M., Ali, Z., Tanveera, M., Aslam, I.: Synthesis of mid-infrared Sn Se nanowires and their optoelectronic properties. Cryst. Eng. Comm. **16**(17), 3470–3473 (2014)
8. Valenzuela, R.: Magnetic ceramics. Cambridge University Press (1994)
9. Zhong, Z., Li, Q., Zhong, Y., Cheng, M., Zhang, Y.: Synthesis of nanocrystalline Ni-Zn ferrite powders by refluxing method. Powder Technol. **155**, 193–195 (2005)
10. Mehar, M.V.K., Bramhachary, P.S., Ramarao, D., Samatha, K.: Structural properties of antimony substituted lithium ferrites sintered at high temperature. IJSRD - Int. J. Sci. Res. Develop. **2**, 2321–0613 (2015)
11. Ateia, E.E., Ahmed, M.A., Salah, L.M., El-Gamal, A.A.: Effect of rare earth oxides and La3+ ion concentration on some properties of Ni-Zn ferrites. Physica B **60-67**, 445 (2014)
12. Rezlescu, E., Rezlescu, N., Popa, P.D., Rezlescu, L., Pasnicu, C.: The influence of R2O3 (R = Yb, Er, Dy, Sm and Ce) on the electric and mechanical properties of a nickel-zinc ferrite. Phys. Status Solidi A **162**, 673–678 (1997)
13. Singh, J.P., Kumar, H., Singhal, A., Sarin, N., Srivastava, R.C., Chae, K.H.: Solubility limit, magnetic interaction and conduction mechanism in rare earth doped spinel ferrite. Appl. Sci. Lett. **2**(1), 3–11 (2016)
14. Nikumbh, A.K., Pawar, R.A., Nighot, D.V., Gugale, G.S., Sangale, M.D., Khanvilkar, M.B., Nagawade, A.V.: Structural, electrical, magnetic and dielectric properties of rare-earth substituted cobalt ferrites nanoparticles synthesized by the co-precipitation method. J. Mag. Mag. Mater. **355**, 201–209 (2014)
15. Ateia, E.E., Abdelatif, G., Ahmed, M.A., Abd Alla Mahmoud, M.: Effect of different Gd^{3+} ion content on the electric and magnetic properties of lithium antimony ferrite. J. Inorg. Organomet. Polym. Mater. **25**, 81–90 (2015)
16. Xu, Z., Yan, S., Barbiellini, B., Harris, V.G., Vittoria, C.: A computational study of nickel ferrite. J. Mag. Mag. Mater. **303**, e432–e435 (2006)
17. Kahn, M.L., Zhang, Z.: Synthesis and magnetic properties of $CoFe_2O_4$ spinel ferrite nanoparticles doped with lanthanide ions. Appl. Phys. Lett. **78**, 3651–3653 (2001)
18. Samha, T.B., Khafagy, R.M., Saleh, N.M.: Promising waste water treatment using rare earth-doped nanoferrites. J. Mag. Mag. Mater. **331**, 256–263 (2013)
19. Geller, S., Gilleo, M.A.: Structure and ferrimagnetism of yttrium and rare-earth-ion garnets. Acta Cryst. **10**, 239 (1957)